JOURNAL OF MATERIALS SCIENCE 27 (1992) 4633–4638

Microdamage and interfacial adhesion in glass bead-filled high-density polyethylene

LU SINIEN, YAN LIN, ZHU XIAOGUANG*, QI ZONGNENG*
*Institute of Mechanics, and *Institute of Chemistry, Zhong Guan Cun Beijing, 100080, People's Republic of China*

The damage mechanism in tensile testing of glass bead-filled high-density polyethylene was studied by *in situ* scanning electron microscopy observation, acoustic emission monitoring and volume dilatation tests. The critical damage stress was measured by micromechanical tests. When the stress field of a multiparticle model has been calculated via Eshelby's method, the interfacial bonding strength can be determined.

1. Introduction

When plastics are used as engineering materials, the mechanical properties frequently do not meet design requirements. Adding second-phase particles to plastics to modify their mechanical properties is a common practice. It has been proved that adding rigid particles to thermoplastics can enhance the elastic modulus substantially [1–4], but the effect of this method on strength and toughness is more complex. It is known that fill-in particulates seems to yield an adverse effect [2, 4, 5, 6]. However, this conclusion may not be universally applicable. We think that the mechanical effect produced by filling-in rigid particles is dependent on the final results incurred by the following two contradictory facts: i.e. one is a strengthening effect which is due to the deformation of the matrix surrounding the particles being constrained by inclusions; the other is a weakening effect which is caused by the filler-incurred damage, and damage may promote the final failure of materials. Therefore, investigation of the mechanisms of microdamage initiation and propagation in materials is vitally important for clarifying the influence of second-phase particles on mechanical properties. Damage induced by particles is affected by many factors, such as shape, size, volume fraction of particles and the physical properties of particles and matrix, etc. Among these factors, nevertheless, interfacial bonding strength is undoubtedly one of the most significant factors. The present work examined the influence of interfacial bonding on various mechanical properties, such as strength, modulus, toughness and creep resistance. By means of *in situ* tensile testing in the scanning electron microscope, acoustic emission, volume dilatation tests and fractographic analysis, the microdamage evolution mechanism in the loading process was also investigated. The critical damage stress of a filled material can be determined by the testing results with calculated stress field of a multi-particle model via Eshelby's method [7, 8].

2. Experimental procedure

2.1. Material

The material investigated is thermoplastic resin filled with rigid spherical particles. High-density polyethylene was selected as the matrix material. Glass beads of diameter 30–40 μm were adopted as the rigid particulate filler. Specimens were manufactured in the Institute of Chemistry, Chinese Academy of Science.

In order to study the effect of interfacial bonding, three types of coupling agent were chosen to make the testing materials (J_4, J_5 and J_6) with different interfacial adhesion. The matrix material, J_0, and the material without using coupling agent, J_1, were taken as reference materials. All details of these materials are shown in Table I.

The interfacial bonding conditions of these materials were determined by the fractograph analysis method. The specimens were dipped into liquid nitrogen and then broken so that the fracture surface could be examined in the SEM. Three different types of fracture surface are shown in Fig. 1a–d. Fig. 2 shows a schematic illustration of crack propagation in the filled materials.

The fracturegraph of J_6, Fig. 1d, illustrates a large number of visible pits and a small number of microbeads whose surfaces are smooth and which have no matrix on them. This indicates that interfacial

TABLE I Experimental materials

	J_0	J_1	J_4	J_5	J_6
Glass bead, V_f (%)	–	10	10	10	10
Coupling agent	–	–	Silane A	Silane B + bismaleimide	Titanate

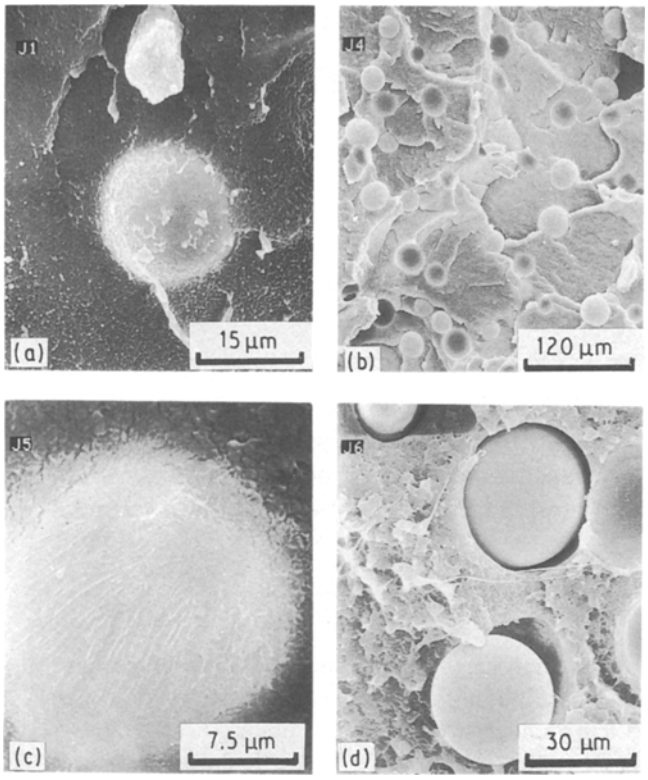

Figure 1 Fractographs of glass bead-filled HDPE with different interfacial adhesion: (a) J_1, (b) J_4, (c) J_5, (d) J_6.

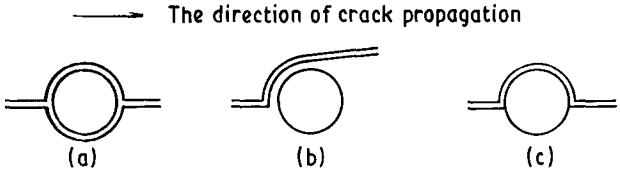

Figure 2 Schematic illustration of crack propagation in filled HDPE. (a) The crack propagates around the particles, separating the particles completely from the matrix. Most of the particles run away from the fracture surface. (b) The crack climbs over the particles. A thin layer of matrix will be left on the particles. (c) The crack propagates over half of the particles. Most particles stay on the fracture surface.

bonding between matrix and particles is very weak, and in the cracking process particles and matrix are completely separated. See Figs 2a and 1d.

The micrograph in Fig. 1c shows that on the fracture surface there are only a few bare particles, and the surface of these particles is covered by a thin layer of matrix substance. This shows that the interfacial bonding is very strong and in the cracking process particles cannot be separated from the matrix, thus the crack has to "climb over" these particles. This can be seen in the schematic drawing of Fig. 2b.

Fig. 1a and b show similar features, where on the fracture surface the number of particles is about the same as that of pits, and some visible debris of matrix is stuck to the surface of the beads. This indicates that the interfacial bonding condition is intermediate between the two above-mentioned materials, J_5 and J_6. The crack propagates over half of the particles, as shown in Fig. 2c.

It can be concluded that J_5 is an excellent adhesive material, J_6 has weak interfacial bonding, and J_1 and J_4 are intermediate in their bonding strengths.

2.2. Equipment

An Instron universal testing machine was used in the tensile tests for the measurements of Young's modulus and strength. Longitudinal and transverse extensometers, were used to measure volume dilatation values in tensile specimens. An acoustic emission instrument model SFS-4 was used to detect the AE signals during tensile process. Creep tests were carried out on a high-performance creep machine which is specially designed for plastics and composites. Creep strain in the gauge length of the specimens was measured by the LVDT set. The *in situ* SEM tensile tests were performed on a tensile stage of a scanning electron microscope model S-570.

3. Results

3.1. *In situ* tensile test on SEM specimens

Small specimens for the tensile tests in the SEM were cut from the standard injection moulding tensile specimens. Their shape and size are shown in Fig. 3. After polishing and coating with gold, the specimens were fixed on the tensile stage of an SEM and extended by tensile loading. A series of photographs was taken at appropriate loading levels. Fig. 4 shows a set of typical microphotographs taken *in situ* of the SEM tensile tests. The photographs indicate that when stress is exerted on the material by loading, the matrix in the polar region of the particles yields and debonds from matrix first, and then as the load increases, the yielding and debonding zone gradually extends (Fig. 4b). Voids appear in the polar zone of the particles (Fig. 4c) growing along the tensile direction. When the load reaches the macroscopic yield strength of the material, the metal layer coated on the matrix breaks and forms a cluster of cracks. This is caused by the large deformation of the matrix in the area between the glass beads (see Fig. 4d). Finally, a shear yielding zone forms (Fig. 4e). At this time the material has lost its load-carrying capacity. All four kinds of particle-filled material in the present paper undergo the above-depicted damage evolution process. The difference between them is that the stress level of the initial debonding differs in each case. For a material with good bonding, such as J_5, the stress level of damage formation and propagation is pronouncedly larger than in other materials.

Experimental observation demonstrates that debonding at the polar region of the particles is in the

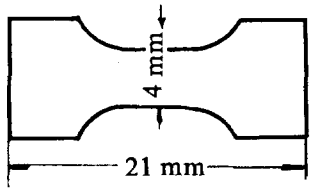

Figure 3 The SEM tensile test specimen.

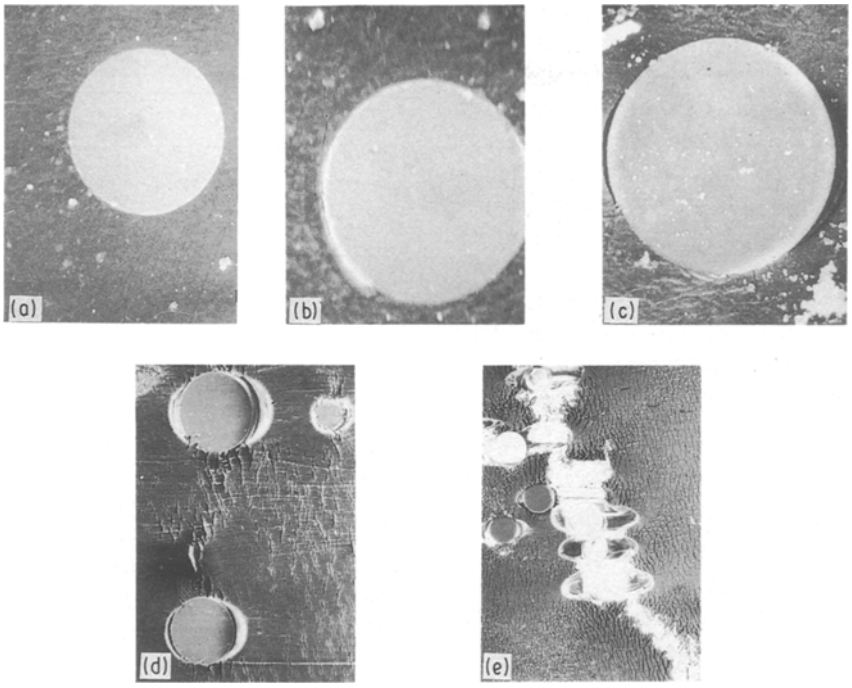

Figure 4 Photographs of *in situ* SEM tensile tested material J_1.

form of initial damage. Hence, the criterion of initial damage can be specified as: when radial stress in the polar region, σ_r^p, reaches its critical value, initial damage occurs, i.e.

$$\sigma_r^p = \sigma_r^{cr} \quad (1)$$

If the mismatch stress of thermal expansion is ignored, σ_r^{cr} can be considered to be the related interfacial bond strength of the material.

Using *in situ* experiments in the SEM, the macroscopic average tensile stress, σ_1, which corresponds to the earliest polar zone debonding, can be measured. The relation between σ_1 and σ_r^{cr} is given by

$$\sigma_r^{cr} = \eta_0 \sigma_1 \quad (2)$$

where η_0 is the stress concentration factor in the polar zone, which can be calculated via computational micromechanics. The computational results will be given in Section 5.

The scatter in the measured values of σ_1 is quite large. The reason for this is that the distribution of microparticles is random and the initial damage may not be detected by the operator. Hence, it is difficult for the value of σ_r^{cr} to be determined exactly by this method. Nevertheless, this approach can reflect the interfacial bond strength qualitatively.

3.2. Acoustic emission monitoring

The occurrence of microdamage in the particle-filled materials, such as cracking, debonding, etc., is inevitably accompanied by a detectable acoustic emission signal. So, using an AE detector to monitor the AE signals emitted in the tensile test or creep process, effective information on the damage evolution process can be acquired.

Figs 5 and 6 show typical AE curves in the tensile tests. Comparison of these two curves shows that

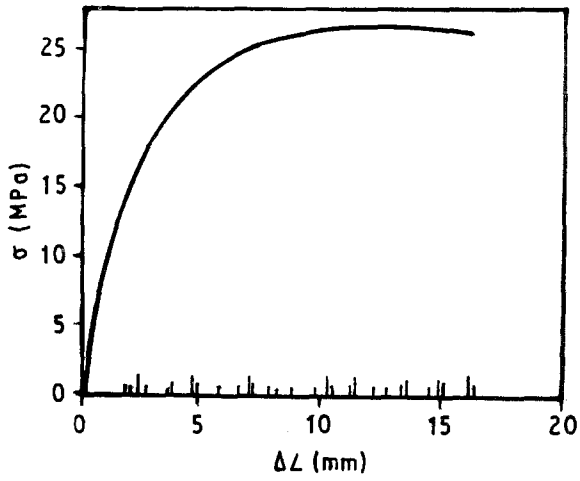

Figure 5 AE events in the tensile testing of material J_5.

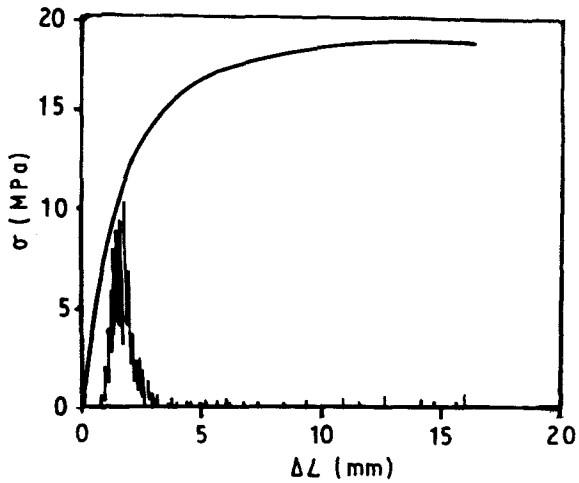

Figure 6 AE events in the tensile testing of material J_6.

a remarkable difference exists in the damage process. The AE curve of excellent adhesion material J_5 indicates that interfacial debonding and cracking processes in the tensile test occur gradually, whereas for the weakly bonded material J_6, an AE peak appears at the lower stress level. After that, the AE signal tends to become stable. This is an indication that debonding of particles from the matrix has already been completed at low stress level.

Further important information can be obtained in the AE diagram, which is the initial AE signal. It is known that the initial AE signal comes from the initial interfacial debonding, thus we have the following relation

$$\sigma_r^{cr} = \eta_0 \sigma_{AE} \quad (3)$$

where σ_{AE} is the stress at onset of the initial AE signal, σ_r^{cr} and η_0 have the same meanings as in Equation 2.

Although the experimental values scatter over a certain range, all the data are fairly stable. The experimental values of σ_{AE} are listed in Table II.

TABLE II σ_{AE} data

	J_1	J_4	J_5	J_6
σ_{AE} (MPa)	7.7–10.1	9.7–11.5	11.0–13.9	7.0–7.5

3.3. Volume dilatation test

During the loading process, cavitation of the material being tested is caused by the microdamage such as cracking, debonding, voids etc. This can be measured quantitatively using a volume dilatation test method.

In tensile tests, the variation of volume dilation, ΔV, can be determined by measurement of longitudinal strain, ε_1, and transverse strain, ε_2, with extensometers.

Experiments demonstrate that until the tensile strain, ε_1, is up to 7%–8%, deformation in the gauge length of specimen is uniform. Hence, within this strain range it is valid for ΔV to be measured using extensometers. Fig. 7 shows the experimental curve of ΔV versus ε_1, where $(\Delta V/V)_R$ is the relative volume variation of particle-filled material to matrix volume variation, i.e.

$$(\Delta V/V)_R = (\Delta V/V)_{filled} - (\Delta V/V)_{matrix} \quad (4)$$

The void ratio inside the material induced by the filling particles can be reasonably characterized by $(\Delta V/V)_R$.

It can be seen that the conditions of interfacial bonding strongly affect the void occurrence process of the material. For instance, at the same strain, ε_1, the void ratio of the material having a strong interfacial bond is notably smaller than that of the material with a weak interfacial bond.

Comparing the experimental results given in Sections 3.1–3.3, it can be deemed that through different surface treatment, the interfacial bond strength of the glass bead-filled high-density polyethylene can be modified to a great extent. Bonding strength between particles and matrix, in turn, influences the damage formation and evolution of the material under loading. These finally affect the mechanical properties of material pronouncedly.

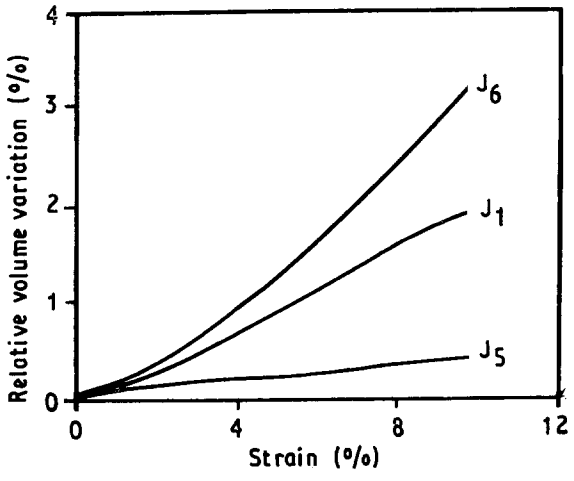

Figure 7 Relative volume variation in tensile tests of filled HDPE.

4. Mechanical properties of tested materials

The modulus, strength and Izod impact values are listed in Table III. It can be noted from the data that filling-in with rigid particles pronouncedly enhances the modulus of the materials. However, the effect of particles on strength depends on the interfacial condition. Strength of material J_5 with excellent adhesion is higher than that of the matrix by 20%. The poor bonding material, J_6 has the lowest strength, and the strength of the intermediate adhesion materials, J_1 and J_4, are approximately the same as that of the matrix. This indicates that strong bonding hinders interfacial debonding and also the void formation processes, and facilitates the strengthening effect in full operation. On the contrary, a weakly bonded interface leads to the premature formation and propagation of microdamage, and thus the weakening effect of particles prevails.

The data for Izod impact strength indicate that although all particle-filled materials have impact values lower than the matrix, the impact value of J_5 with strong interfacial bonding is the highest of the four particle-filled materials. This can also be explained reasonably from the view point of microdamage.

Fig. 8 shows a set of creep curves. The creep stress selected corresponds to about 50% of the yield stress of the matrix. Hence, as creep proceeds, microdamage will occur in the particle-filled materials. The data indicate that the creep resistance of material J_5 is remarkably higher than that of the matrix J_0, revealing that the strengthening effect is also sustained by strong interfacial bonding. However, weak interfacial bonding notably reduces the creep resistance of material J_6.

TABLE III Mechanical properties data

	J_0	J_1	J_4	J_5	J_6
σ_s (MPa)	21.8	21.4	21.4	26.2	18.3
E (GPa)	0.88	1.16	1.05	1.09	0.82
Izod notch impact (J cm^{-1})	2.58	0.64	0.77	1.49	1.01

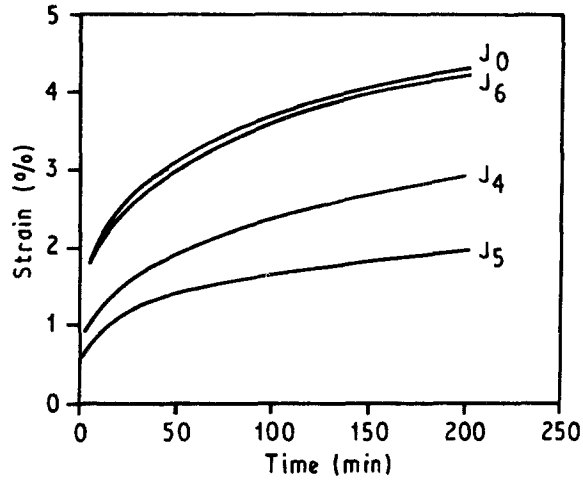

Figure 8 Creep curves of filled HDPE, with σ = 12 MPa.

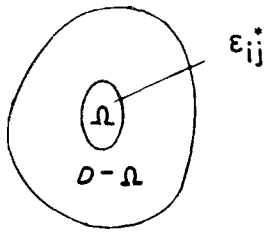

Figure 9 Inclusion Ω.

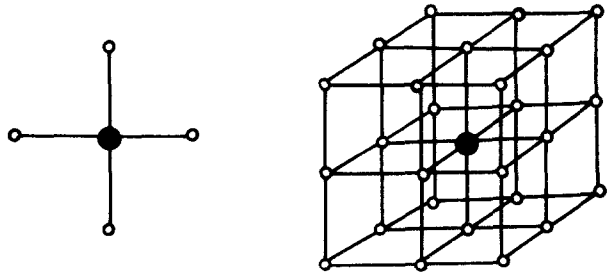

Figure 10 The five-particle and 27-particle models.

5. Calculation of the stress field of microparticle inclusions

Eshelby gave the solution of eigenstrains for an elastic field caused by an inclusion. It is expressed as follows. Consider an ellipsoidal inclusion, Ω, which contains eigenstrains ε_{ij}^* in an isotropic infinite body (see Fig. 9); both strain disturbances for the interior and exterior of Ω can be expressed by

$$\left.\begin{aligned} \varepsilon_{ij}^c &= S_{ijkl}\varepsilon_{kl}^* \quad \text{in } \Omega \\ \varepsilon_{ij}^c(x) &= D_{ijkl}(x)\varepsilon_{kl}^* \quad \text{in } D - \Omega \end{aligned}\right\} \tag{5}$$

where S_{ijkl} and $D_{ijkl}(x)$ are Eshelby's tensor and generalized Eshelby's tensor [7].

The stress field can be obtained using Hook's law

$$\left.\begin{aligned} \sigma_{ij}^0 + \sigma_{ij}^c &= C_{ijkl}(\varepsilon_{kl}^0 + \varepsilon_{kl}^c) \quad \text{in } D - \Omega \\ \sigma_{ij}^0 + \sigma_{ij}^c &= C_{ijkl}^*(\varepsilon_{kl}^0 + \varepsilon_{kl}^c) \quad \text{in } D \end{aligned}\right\} \tag{6}$$

where σ_0, ε_{kl}^0 are the stress and strain field in $D - \Omega$ caused by an applied stress σ_{ij}^∞, σ_{ij}^c, ε_{kl}^c are the stress disturbance and strain disturbance caused by the inclusion. C_{ijkl}, C_{ijkl}^Ω are the elastic modulus of the body and inclusion, respectively.

The equivalent inclusion equation can be written as

$$C_{ijkl}^\Omega(\varepsilon_{kl}^0 + \varepsilon_{kl}^c) = C_{ijkl}(\varepsilon_{kl}^0 + \varepsilon_{kl}^c - \varepsilon_{kl}^*) \tag{7}$$

If finite inhomogeneous inclusions $\Omega_1, \Omega_2, \ldots, \Omega_k, \ldots, \Omega_n$ are contained, and their Young's moduli are $C_{ijkl}^1, C_{ijkl}^2, \ldots, C_{ijkl}^k, \ldots, C_{ijkl}^n$, the equivalent equation of inclusion k is

$$C_{ijkl}^k(\varepsilon_{kl}^0 + \varepsilon_{kl}^{ck}) = C_{ijkl}(\varepsilon_{kl}^0 + \varepsilon_{kl}^{ck} - \varepsilon_{kl}^{*k}) \quad \text{in } \Omega_k \tag{8}$$

The strain disturbance caused by all inclusions can be written as

$$\varepsilon_{kl}^{ck} = \sum_{\substack{s=1 \\ s\neq k}}^{n} D_{ijkl}^s(x)\varepsilon_{kl}^{*S} + S_{ijkl}\varepsilon^{*k} \quad \text{in } \Omega_k \tag{9}$$

From Equations 6, 8 and 9, ε_{ij}^{*k}, ε_{ij}^{ck} and then σ_{ij}^c can be obtained.

In this paper, the five-particle model and 27-particle model shown in Fig. 10 were solved [8]. Mori-Tanaka's assumption [9] was employed to take the multi-inclusion effect into account. The stress distribution around particles was obtained through calculation. They are given in Figs 11 and 12. The results show that radial stress reaches a maximum value at the polar region. With 10% volume fraction of particles, the value of $\eta_0 = 1.76$, and $\eta_0 = 1.70$ when $V_f = 3\%$.

If the mismatch stress of thermal expansion is ignored, σ_r^{cr} can be acquired by using an average value of σ_{AE} in Table II and a calculated value of η_0. This is shown in Table IV. The data in Table IV indicate that σ_r^{cr} of poor bond material J_6 is about 60% of the yield stress, σ_s of the matrix, and that of the excellent adhesion material J_5 is approximately equal to the σ_s of the matrix. According to the calculated results of stress distribution around the particles, it can be proved that the von Mises yield criterion is not satisfied in material J_6 when the tensile stress reaches σ_{AE}. Thus the matrix will not yield when debonding occurs. This conclusion agrees with SEM observations. With J_5, the combination of stresses in the region of $0° \leqslant \theta < 60°$ (see Fig. 13) reaches the critical value of von Mises criterion before the particle debonds from the matrix. However, plastic deformation of the matrix can be observed only at some local microareas, because the deformation of the matrix surrounding the particles is constrained by the rigid inclusions.

TABLE IV Value of σ_r^{cr}

	J_4	J_5	J_6
η_0	1.76	1.76	1.76
σ_r^{cr}	18.7	21.9	12.8

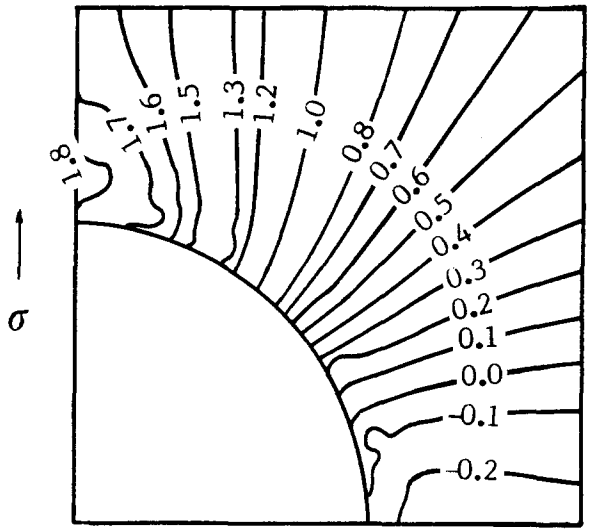

Figure 11 The isoline of σ_r/σ_{ave} around a glass bead, $V_f = 10\%$, $n = 27$.

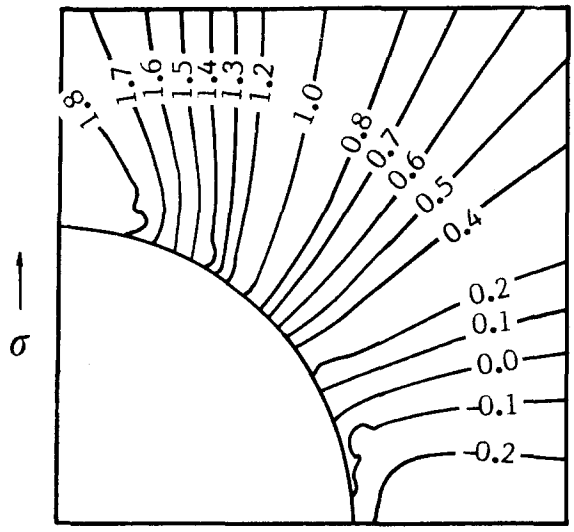

Figure 12 The isoline of σ_r/σ_{ave} around a glass bead, $V_f = 10\%$, $n = 5$.

6. Conclusions

1. Addition of particles to a matrix produces a large turbulence of stress distribution, leading to microdamage inside the materials. This value of interfacial bonding strength between particles and matrix strongly affects the process of damage initiation and evolution, and thereby significantly influences the mechanical properties of the materials.

2. Materials with excellent interfacial adhesion are superior in their strength, modulus and creep resistance to the matrix materials. Izod impact values of the well-bonded materials are also higher than those of weaker bonded materials, and can reach as much as 60% of that of matrix. Therefore, proper choice of coupling agent can render particulate-filled materials with better comprehensive mechanical properties.

3. By using macromechanical property measurement, combined with microdamage monitoring and micromechanics analysis, reasonable results of interfacial bond strength can be obtained.

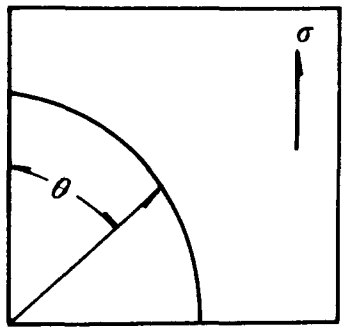

Figure 13 Unit cell for a sphere-filled composite.

Acknowledgement

This project was supported by the Chinese National Natural Science Foundation.

References

1. J. LAHILI and A. PAUL, *J. Mater. Sci.* **20** (1985) 2253.
2. U. YILMAZER and R. J. FARRIS, *Polym. Compos.* **4** (1983) 1.
3. L. NICOLAIS, G. GUERRA, C. MIGLIARESI, L. NICODEMO and A. T. DI BENEDETTO, *Composites* **12** (1981) 33.
4. M. E. J. DEKKERS and D. HEIKENS, *J. Appl. Polym. Sci.* **28** (1983) 3809.
5. D. L. FANLKNER and L. R. SCHMIDT, *Polym. Engng Sci.* **17** (1977) 657.
6. A. G. EVANS, *Phil. Mag.* **26** (1972) 1327.
7. T. MURA, "Micromechanics of Defects in Solid" (Nijhoff, The Hague, 1982).
8. YAN LIN, Master thesis Institute of Mechanics, Chinese Academy of Science, China (1990).
9. A. N. NORRIS, *J. Appl. Mech.* **56** (1989) 83.

Received 19 March
and accepted 12 December 1991